

A Comparative Study: Seismic Deformability and Strength of Non-conforming Columns



F. Dameh and S. J. Pantazopoulou

1 Introduction

It has been observed in reconnaissance reports following previous strong ground motion events that many structural components constructed prior to the introduction of modern seismic design concepts (e.g. before the 1980's in the Western world) exhibit premature failures which prevent these components from developing their intended full deformation capacity and strength [15]. Structural deficiencies may be associated with substandard detailing and dimensioning that was mainly based on allowable stress design with no emphasis on the confining function of adequately anchored stirrups. Therefore, substandard R.C buildings may collapse due to localization of failure in few locations of the building prior to redistribution of stresses [2, 5, 9, 11]. Premature mechanisms leading to localized failures may include buckling of compression reinforcement, slip of longitudinal reinforcement due to the presence of poorly confined lap splices in the plastic hinge zone region-which was a common practice more than 40 years ago-, crushing of concrete in the member web, etc.). Those types of structural components which do not comply to modern seismic provisions are labeled henceforth nonconforming members [7].

Nonconforming members exist in a large number of concrete structures across Canada. They are a result of older methods of construction prior to the earthquake engineering community worldwide could reach a thorough understanding of the mechanics of seismic resistance of RC; such structures are deemed unsafe according to current building codes [14]. Therefore, there is a need for improved understanding of the critical mechanisms governing the deformation capacity and strength of RC structures, along with better calibration of the prevalent assessment model.

F. Dameh (✉) · S. J. Pantazopoulou
York University, Toronto, Canada
e-mail: Fardam96@yorku.ca

2 Analytical Models

Using an advanced finite element software (ATENA V.5 3D Engineering) a series of benchmark columns are modeled considering different effects of detailing representing nonconforming construction [4]. All columns are subjected to monotonic loading. Using ATENA Studio (ATENA Studio $\times 64V.5.6.1. 17,830$) the resistance curves for the columns were calculated and the deformation and strength capacities were recorded to form a data base for a comparative study. Figure 1a presents the five different cases of column models considered, with differences in longitudinal reinforcement detailing: (1) The longitudinal reinforcement bars are fully anchored into the foundation with a 90° hook, (2) Bars are lap spliced over a lap length of $15D_b$, (3) Bars extend into the foundation with an anchorage length of $15D_b$, (4) The column has a deep cross Section (700 mm depth), (5) A hinge is fabricated at the base of the column—where the longitudinal reinforcement crosses the center of the cross section and therefore produces a zero moment point. Each case of longitudinal detailing shown in Fig. 1a is modeled with different combinations of axial loading (10, 35, 50% of crushing), longitudinal reinforcement (shown in Fig. 1b) and stirrup spacing (100- and 200-mm stirrup spacing) with 8 mm stirrup diameter. The column identification code is as following: The first numeral following the letter C (for Column)—for example C35—corresponds to the normalized axial load ratio applied to the columns which in this case is 35% of the crushing load, followed by the section ID number (each section contains a different amount of longitudinal reinforcement, so as to control the hierarchy between flexural and shear demands as shown in Fig. 1b) whereas the last number digit in the numeral represents the stirrup spacing in cm along the length of the shear span of the column.

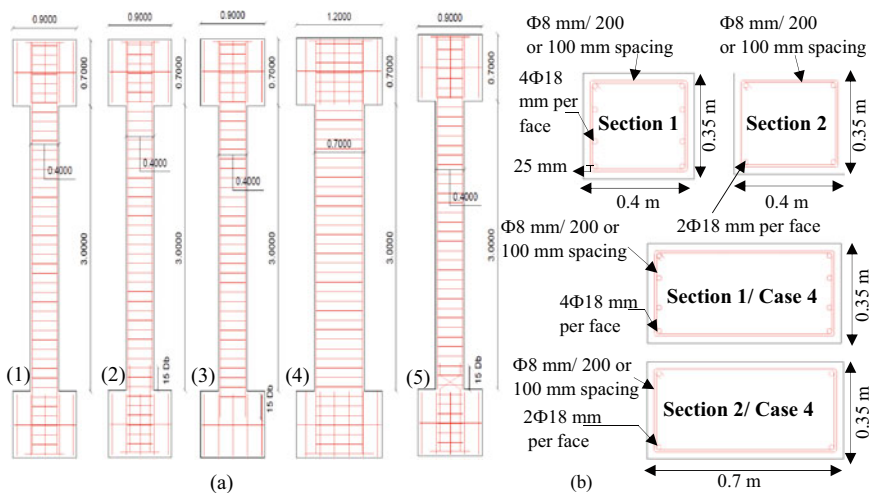


Fig. 1 a Column cases and detailing (all dimensions are in m). b Section geometry

The columns are modeled using 3D macro elements. The columns have a clear length of 3 m. The foundation is modeled as a block with dimensions (0.9 × 0.9 × 0.7) m. A symmetrical beam block is assumed at the top to enable application of lateral load. The dimensions of the foundation are increased for case 4 to (1.2 × 1.2 × 0.7) m.

2.1 Finite Element Model

The cases in Fig. 1a were modeled using a laterally swaying cantilever model with a shear span length equal to half of the column's deformable length ($3/2 = 1.5$ m). Moreover, due to symmetry half the cross section was modeled. The columns were discretized into 3D brick elements (8 noded) with a brick size ranging between 0.025 m for the bottom portion of the column (0.5 m) and 0.05 m for the rest of the column. The reinforcement is modeled through 1D reinforcement truss elements. The columns were modeled with a stiff steel plate on the top and side of the column to eliminate localized failure when applying axial and lateral loads. The axial load was applied in the first analytical step followed by monotonic steps of 0.4 mm lateral displacement until columns would completely fail. The bottom surface nodes of the foundation are restrained from movement in x, y and z directions. The section's symmetrical plane was restrained from movement in the x-direction (the direction perpendicular to the symmetrical plane). Two monitor points were placed at the point of lateral displacement application. One for recording the reactions and one for displacements. The reported reactions represent the entire cross section. Therefore, the load-displacement (monotonic resistance envelopes) are obtained.

2.2 Material Models

2.2.1 Concrete and Reinforcement Stress-Strain Relationships

NonlinearCementitious2 User material was used to model concrete behaviour. This model uses a combination of plasticity and fracture relationships to simulate the full range of inelastic stress-strain behavior of concrete [3]. The cracked stiffness in this model was calculated using the help of the retention shear factor r_g as described in Eq. 1, whereas the strain value in tension or compression is calculated in this model as shown in Eq. 4 [3].

$$E'_{ijij}{}^{cr} = r_g \cdot G / (1 - r_g) \quad (1)$$

$$G = r_g \cdot G_c \quad (2)$$

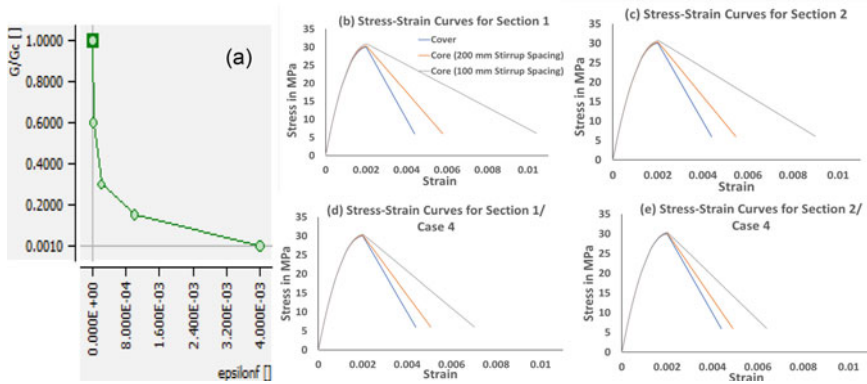


Fig. 2 Concrete stress strain curve for different sections and transverse stirrup spacing

$$G_c = E_c/2 \cdot (1 + \nu) \quad (3)$$

$$\text{If } \epsilon_1^f < \epsilon_{loc}^f, \quad \epsilon = \epsilon_1^f \quad \text{else} \quad \epsilon = \epsilon_{loc}^f + (\epsilon_1^f - \epsilon_{loc}^f) \frac{L_t}{L_{ch}^t} \quad (4)$$

In the above, E_{ijij}^{cr} is the cracked stiffness, r_g is the minimum of the shear retention factor on cracks in both directions i and j , G is the elastic shear modulus, and the retention shear factor is defined in Fig. 2a. L_{ch}^c and L_{ch}^t in Eq. 4 represent a size for which the diagram in tension and compression is valid and decreases the dependency on the mesh [3]. For the column models 0.03 and 0.050 m are used for L_{ch}^c and L_{ch}^t respectively with trial and error so as to capture an appropriate response. L_t and L_c represent the crack band size and crush band size respectively. Parameter ϵ is the strain tensor at the finite element integration points. The localized softening strain in compression is defined as the strain corresponding to the maximum compressive strength after subtracting the linear portion of the stress strain curve [3]. The localized softening strain in tension is assumed 0 for plain concrete thus no hardening occurs after the first crack initiates [3]. Concrete compressive strength for the unconfined concrete used is $f_c = 30$ MPa, $E_c = 30,000$ MPa and $\nu = 0.2$. The stress strain curve of concrete was determined based on Hognestad's parabola [8] for the ascending branch. Kent and Park [10] softening branch model was used to model the concrete cover. Modified Park and Kent [16] was used to model the confined core. The stress strain relation for concrete is shown in Fig. 2 for all cases of longitudinal and transverse reinforcement ratios. The mechanical properties used for transverse and longitudinal reinforcement are listed in Table 1.

Table 1 Longitudinal and transverse reinforcement properties

	Longitudinal reinforcement: (ASTM A706 grade 60 ksi)	Transverse reinforcement: (ASTM A615 grade 40 ksi)
Yield strength	414 MPa	276 MPa
Ultimate strength	552 MPa	483 MPa
Strain rupture	120 mm/m	120 mm/m

2.2.2 Reinforcement Bond

The longitudinal reinforcement is connected to the concrete through interface springs endowed with a proper bond stress-strain relationship to allow the slip between the bar and concrete. In this manner pullout or splitting behavior of the longitudinal reinforcement can be considered. The bond stress-slip relationship was determined based on fib Model Code 2010 [13] assuming good bond conditions. Splitting failure is estimated to occur along the shear span of the column. For the case of 100 mm stirrup spacing the maximum bond strength was used as shown in Eq. 5. However, in the case of 200 mm stirrup spacing the unconfined maximum bond stress was used as shown in Eq. 6, as the effective confining pressure in this case is, $K_e < 0.3$. Equation 7, 8, 9 and 10 are used to calculate the milestone points of the bond-slip relationship. Bond strength T_{max} is calculated as $2.5 \sqrt{f_c}$. The residual strength for the 100 mm stirrup spacing case is $0.4 * T_{max}$. A value of 0 is assumed for the residual strength for lower confinement according to the code. The bond stress-slip relation used for the column models are shown in Fig. 3.

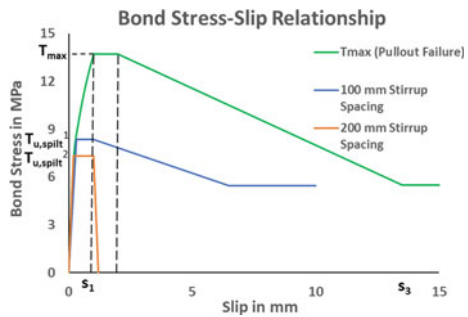
$$T_{u,split}^1 = 8 \cdot (f_c/25)^{0.25} \tag{5}$$

$$T_{u,split}^2 = 7 \cdot (f_c/25)^{0.25} \tag{6}$$

For slip calculations:

$$T_o = T_{max} \cdot (s/s_1)^{0.4}, \text{ for } 0 \leq s \leq s_1 \tag{7}$$

Fig. 3 Bond stress-slip relationship



$$T_o = T_{\max}, \text{ for } s_1 \leq s \leq s_2 \quad (8)$$

$$T_o = T_{\max}(T_{\max} - T_f) \cdot (s - s_2) / (s_3 - s_2), \text{ for } s_2 \leq s_3 \quad (9)$$

$$T_o = T_f, \text{ for } s_3 < s, \text{ where, } T_{\max} = 2.5 \cdot f_c^{0.5} \quad (10)$$

3 Results and Analysis

3.1 Deformation and Strength Capacities and Modes of Failure for Cantilever Models

Table 2 displays the deformation capacities and strengths for each case shown in Fig. 1a. The strength is plotted against the drift ratios (which is defined as the displacement divided by the length of the shear span (1.5 m)) as shown in Fig. 4. To make a fair comparison of the different resistance curves in order to reveal the influence of the parameters studied, the apparent loss of lateral load resistance owing to P- Δ effect was eliminated in the plots by adding the product of the axial load multiplied by the drift ratio at each point. Figure 5 depicts the failure of the columns under ultimate loading capacity.

4 ASCE/SEI 14/17 and Eurocode 8-Part III 2005 Deformation Capacity Correlation

The deformation capacities at different performance stages using the ASCE/SEI 14/17[1] and Eurocode 8 III 2005 were calculated. The performance levels are determined in the codes at Near Collapse (NC), Significant damage (SD) and damage limitation (DL) performance limit states in the Eurocode 8 [6] which correspond to Collapse prevention (CP), Life safety (LS), Immediate Occupancy (IO) respectively in the ASCE/SEI 14/17. Figures 6a, b and c plots the 3 limit stages according with the ASCE/SEI 14/17 plotted against the model analytical data. Similarly, Fig. 6d, e and f illustrates the performance levels in the Eurocode 8 III [6] plotted against the model data.

Figure 5 depicts the mode failures of the columns. Where Fig. 5a is for set 1, b is for set 2, c is for set 4, and e is for set 5.

Table 2 Deformation and strength capacities for 5 different columns

Axial load (%)		100 mm stirrup spacing				200 mm stirrup spacing							
		4 Φ 18 bars per face		2 Φ 18 bars per face		4 Φ 18 bars per face		2 Φ 18 bars per face					
		Shear force (KN)	Δ_y mm	Δ_u mm	Shear force (KN)	Δ_y mm	Δ_u mm	Shear force (KN)	Δ_y mm	Δ_u mm			
Set 1 (full anchorage in foundation with 90° hook)													
10		153.12	9.8	43.6	107.01	7.8	55	153.5	9.4	37	106.54	7.4	38.7
35		242.96	11.2	42.3	194.47	8.8	33	237.5	10.4	23.6	192.14	8.5	21
50		261.17	10.6	31	212.65	8.2	25	246.49	8.8	19.4	205.6	7	17
Set 2 (lapped splice-270 mm lap length)													
10		146.63	12.2	26	104.64	10.2	36.2	143.64	11.2	17.2	103.01	9	26
35		224.60	11.5	38.8	181.81	8	34	211.13	9.1	22	173.31	6.8	20.2
50		233.82	9	31	192.81	7	25.5	223.46	7.8	15.8	185.83	6.5	15.2
Set 3 (short anchorage length)													
10		142.86	9	30.8	106.7	7.8	52.3	137.22	7.9	15	106	7.5	41
35		238.53	11	33.5	194.08	9	32	231.72	10	20.8	192.9	8.4	21.7
50		259.46	10.7	31	211.48	8.3	25.3	246.35	8.8	19.6	205.31	7.3	17.5
Set 4 (deep cross section)													
10		361.08	5.7	35	265.9	4	35.8	356.8	5.3	28.5	266.26	3.8	28.3

(continued)

Table 2 (continued)

Axial load (%)	100 mm stirrup spacing				200 mm stirrup spacing							
	4 Φ 18 bars per face		2 Φ 18 bars per face		4 Φ 18 bars per face		2 Φ 18 bars per face					
	Shear force (KN)	Δ_y mm	Δ_u mm	Shear force (KN)	Δ_y mm	Δ_u mm	Shear force (KN)	Δ_y mm				
35	638.14	6.3	23	549.71	5.5	20	625.37	5.9	17	544.51	5.1	15.1
50	704.5	6	15.5	608.94	5.2	14.2	673.8	5.5	11	588.46	4.8	11.2
Set 5 (hinge connection to the foundation base)												
10	82	8	53	70.71	6	44.8	77.75	6	41.6	68.35	4.8	47.5
35	161.36	5.5	39	153.34	5.5	30	159.39	5.4	21.5	152.04	5.2	19.8
50	190.51	6.2	28	179.48	6	20	185.99	5.8	14.8	175.99	5.8	13.4

Note The shear force is the maximum resistance attained by the column. Δ_y is the effective yield displacement found using ASCE/SEI 14/17 code standards. Δ_u is the displacement at 15% reduction in shear force on the post peak resistance curve

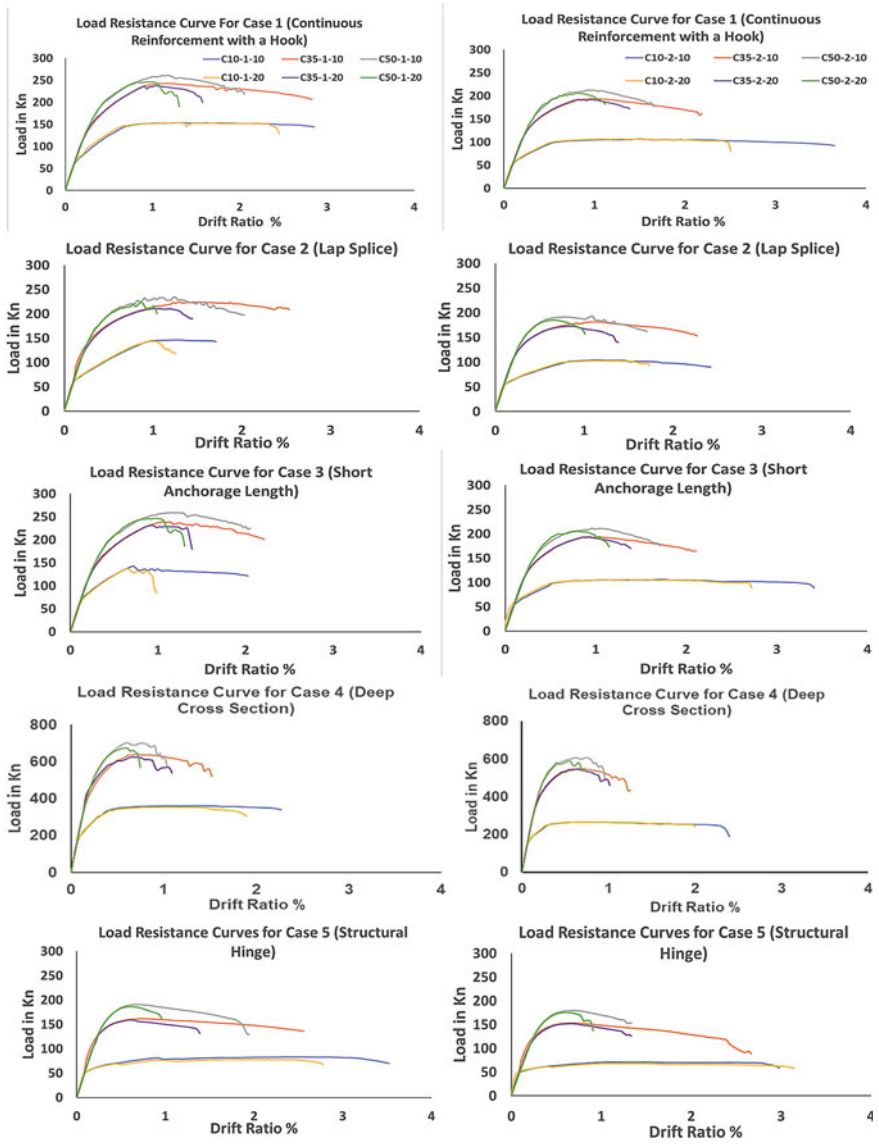


Fig. 4 Load-displacement for all cases of longitudinal reinforcement. Here, the drift ratio is defined as the displacement of the column divided by the column's shear span length

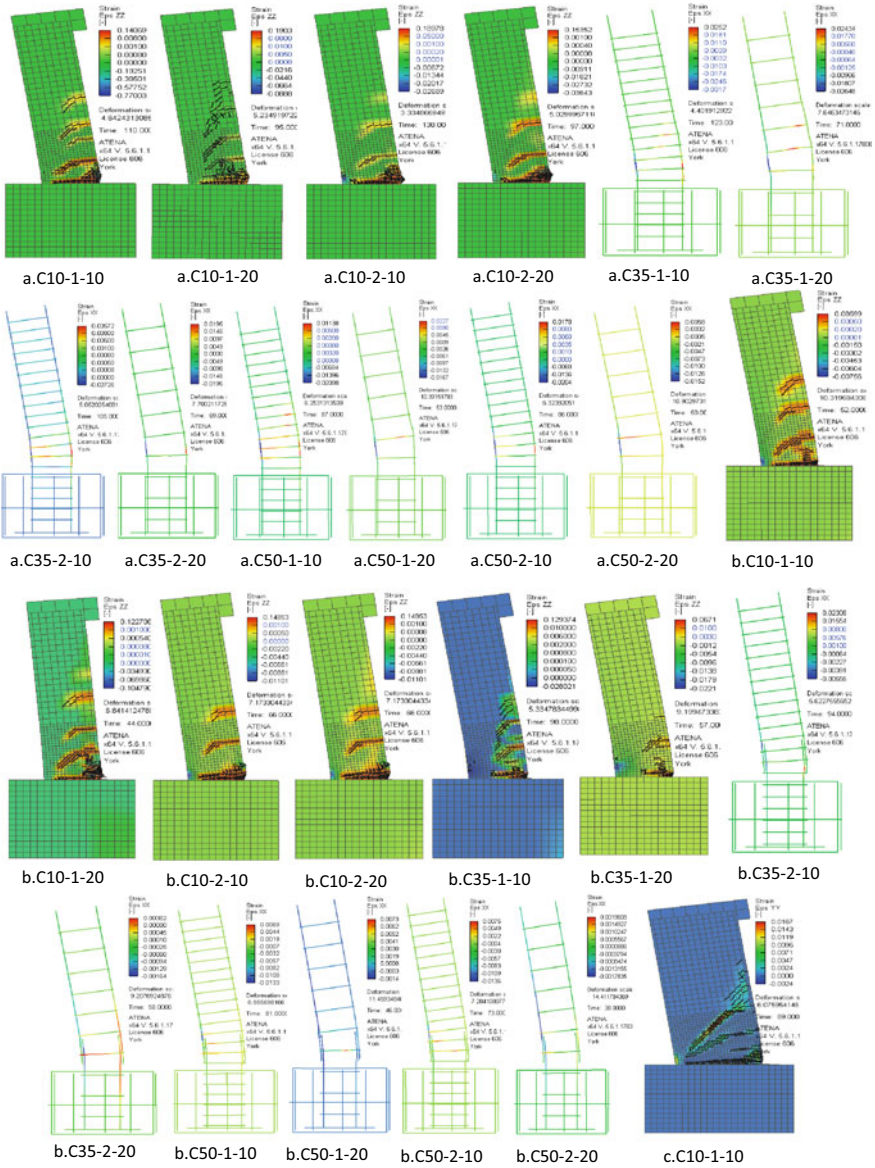


Fig. 5 Column failure modes at near collapse state. Strain XX are the longitudinal strains in reinforcement and strain ZZ are the strains in concrete

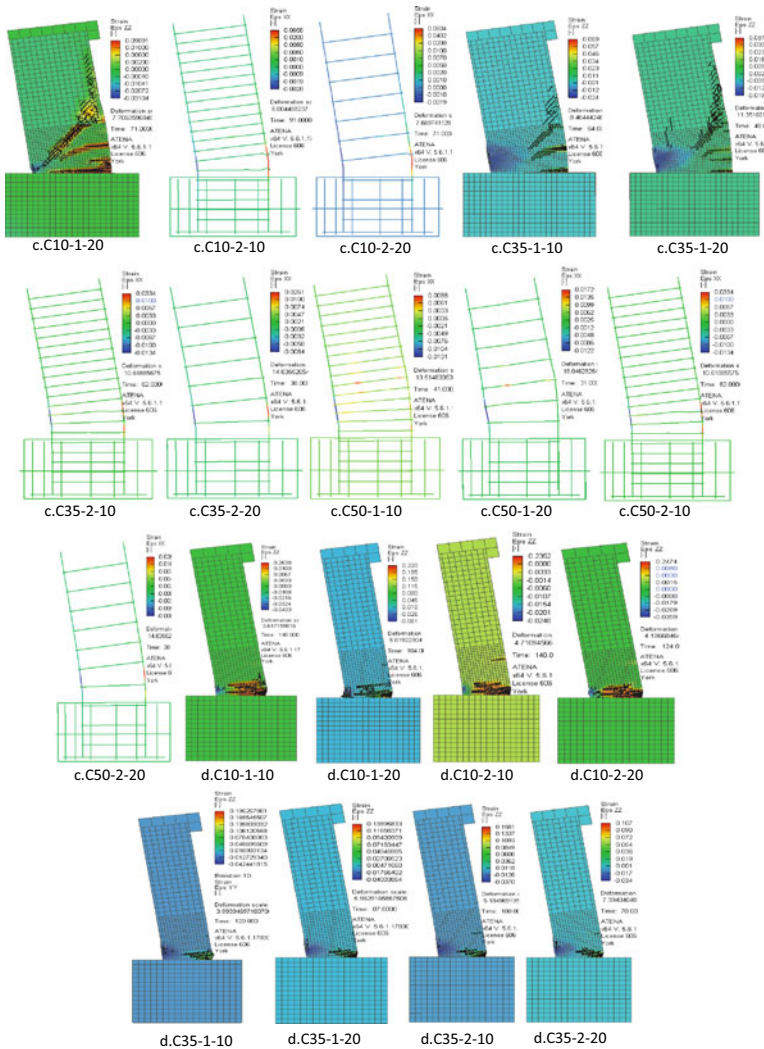


Fig. 5 (continued)

5 Discussion and Conclusions

This study investigated the deformation capacity and its correlation to the assessment codes at three performance levels (acceptance criteria). Columns with well confined stirrups provided larger deformation capacities. The column's shear strength started to vary at high axial loads, indicating stirrup yielding and shear failure. Moreover,

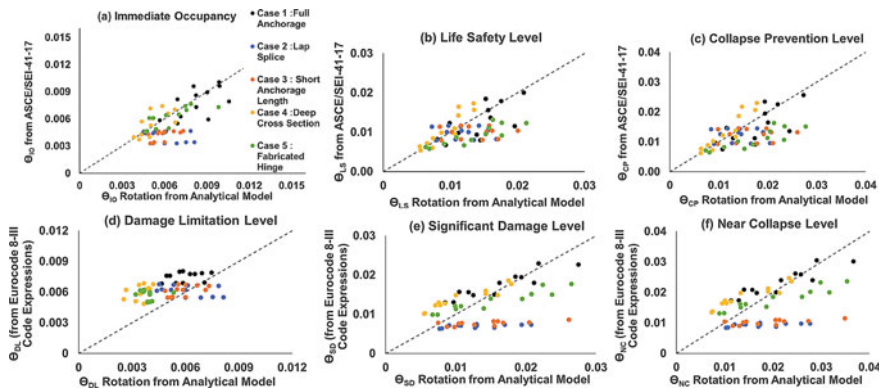


Fig. 6 Code estimated rotation capacities vs. values from F.E. Models **a–c** Limit states from ASCE/SEI 41-17; **d–f** Limit states from Eurocode 8-III

it was found that the effective yielding increased with the increase of the axial load. A decrease in the effective yielding at an axial load of 50% was found due to the occurrence of concrete crushing failure. The hinge fabrication at higher axial loads was excluded from this behaviour as reinforcement slips were present at lower axial loading. Moreover, column yielding was delayed at low axial loads in the case of lap spliced column. This is due to the delay in the longitudinal reinforcement yielding due to the increase of slip. It is also concluded that the column's deformation capacities decrease with an increase in the axial loads. Columns with low axial load failed due to splitting. The crushing of concrete is also present at 50% crushing load, limiting longitudinal bar yielding especially in the cases of low confinement. The effect of the longitudinal reinforcement detailing present in the lap splice and short anchored reinforcement was attenuated with the increase of the compressive loading. Thus, the reinforcement slip from the foundation was mitigated when lateral displacements were applied. At lower axial load stronger deterioration of ultimate deformation capacities occurred as these columns were dominated by the pullout slip of the reinforcement. It should also be noted that the pullout demand in these cases for columns lightly reinforced are less affected. This was observed due to the prevalence of flexural yielding. For deep cross sections, the larger internal lever arm also increased the shear demand. Shear failure could occur at lower shear strengths with lower deformation capacities.

The ASCE/SEI 41-17 procedures showed better correlation to the rotation at yielding when compared to deformation capacities from models as opposed to the Eurocode 8 III [6]. This is because shear force demands are considered in calculating the rotation capacities in the ASCE/SEI 41-17. For the second set (the lapped splice), the finite element models show a decrease in the yield rotation compared to columns in the first set (columns with continuous reinforcement). This increase is attributed to the increase of slip rotations along the reinforcement bar. However, this is not reflected in the assessment codes properly. The codes demand a decrease in the slip rotation in a lapped splice column at yielding compared

to columns with full anchorage. Generally, the assessment codes show a decrease in the life safety/significant damage state with the increase of the axial load for all column cases. However, from the finite element models it was found that this trend was not applicable to columns that fail ultimately due to reinforcement slips, which are columns in set 2 and 3 (lapped splice and short anchorage length) that have high reinforcement ratios. This is because the compression forces of the axial load mitigate the pullout forces when applying lateral load. In the case of 50% the ultimate rotations decrease, as the column were controlled by concrete crushing rather than pure slip. At Near Collapse or Collapse Limit state the scatter increased when the column was controlled by crushing of concrete according with the Eurocode at higher axial loads. However, according with the ASCE SEI 14/17, values successfully matched the calculated ones in computing the deformation capacities when concrete crushing failure controlled. The Eurocode 8 III [6] showed lesser correlation to the computational results for columns failing ultimately in buckling/shear.

References

1. ASCE-41-17 (2017) ASCE standard, ASCE/SEI, 41-17: seismic evaluation and retrofit of existing buildings. American Society of Civil Engineers, Reston
2. Augenti N, Parisi F (2010) Learning from construction failures due to the 2009 L'Aquila, Italy, earthquake. *J Perform Construct Facil* 24(6):55–536
3. Cervenka V, Jendele L, Cervenka J (2020) Theory. ATENA program documentation part 1. Cervenka Consulting, Prague
4. Chassioti SG, Syntzirma DV, Pantazopoulou SJ (2010) Codes of assessment of buildings: a comparative study. In: 9th US National and 10th Canadian conference on earthquake engineering 2010, including papers from the 4th international Tsunami symposium, vol 2, pp 1192–1201
5. Dogangun A (2004) Performance of reinforced concrete buildings. *Eng Struct* 26(6):841–856
6. EN 1998-3 (2005) Eurocode 8—design of structures for earthquake resistance—part 3: assessment and retrofitting of buildings. European Committee for Standardization (CEN), Brussels
7. FEMA 356 (2000) Pre-standard and commentary for the seismic rehabilitation of buildings
8. Hognestad E (1951) A study of combined bending and axial load in R.C. members. University of Illinois Engineering Experiment Station. Bulletin no. 399
9. Jeong SH, Elnashai AS (2004) Analytical and experimental seismic assessment of irregular RC buildings. In: 13th world conference on earthquake engineering, Vancouver, Canada
10. Kent DC, Park R (1971) Flexural members with confined concrete. *J Struct Div ASCE* 97(ST7):1969–1990
11. Lang AF, Marshall JD (2011) Devil in the details: success and failure of Haiti's non engineered structures. *Earthq Spectra* 27(S1):72–345
12. Lehman DE, Calderone AJ, Moehle JP (1998) Behavior and design of slender columns subjected to lateral loading. In: 6th US National conference on earthquake engineering, EERI, Seattle, Washington, 31 May–04 June 1998
13. Model Code 2010: final draft, fib—Bulletin 65, vol 1. www.fib-international.org.
14. National Research Council of Canada (1995) Guideline for seismic upgrading of building structures upgrading of building rehabilitation. Institute for Research and Construction NRC Publications Archive

15. Pantazopoulou SJ (2003) Strength and deformation capacity of non-seismically detailed components. Seismic assessment and retrofit of reinforced concrete buildings, fib Bulletin No. 24:91–150
16. Park R, Priestley MJN, Gill WD (1982) Ductility of square-confined concrete columns. J Struct Div 108:929–950